Available online at www.sciencedirect.com
SCIENCE DIRECT®
Journal of Nuclear Materials 340 (2005) 291–298
journal of nuclear materials
www.elsevier.com/locate/jnucmat

The response of several luminescent materials to keV and MeV ions

Kieran J. McCarthy [a,*], J. García López [b], D. Jiménez Rey [a], B. Zurro [a], A. Ibarra [c], A. Baciero [a], M.A. Respaldiza [b]

[a] Laboratorio Nacional de Fusión, Asociación Euratom-CIEMAT, Avenida Complutense 22, E-28040 Madrid, Spain
[b] Centro Nacional de Aceleradores, Parque Tecnológico, 'Cartuja '93', Avenida Thomas A. Edison, E-41092 Seville, Spain
[c] Materiales para Fusión, Asociación Euratom-CIEMAT, Av. Complutense 22, E-28040 Madrid, Spain

Received 20 October 2004; accepted 7 December 2004

Abstract

We have quantified the ionoluminescence of several materials when irradiated with protons and He ions accelerated to keV and MeV energies. In particular, we have determined the absolute luminosity in terms of the number of photons emitted per incident ion from the front and back faces of thin screens of $Y_3Al_5O_{12}$:Ce (0.15% CeO_2), Al_2O_3:Ti (0.2% Ti), fused silica, and chemical vapour deposited diamond. This work has been motivated principally by their application in diagnostics for measuring fast ion losses at the edges of hot plasmas in fusion devices, where their radiation hardness, compared to that of standard phosphors, make them attractive candidates. Here, after presenting brief descriptions of the materials and summarizing the experimental set-up and the analysis method used, the results obtained are presented, and the afterglow and damage are evaluated.

PACS: 78.60.Hk; 52.70.−m; 29.17.+w; 87.50.Gi

1. Introduction

Several decades of research on phosphors at CERN and elsewhere have led to the use of doped alumina ceramic screens, e.g. Al_2O_3:Cr^{3+} [1,2] and Ce-doped YAG single crystal converters [3] for accelerator beam (electrons and ions) observations. In particular, such screens exhibit good response linearity and good relative sensitivity to charged particles accelerated to MeV and GeV energies. Furthermore, the immunity of such phosphors to electromagnetic interference and ground loops, as well as their compactness (only a thin screen is required), makes them well suited for use as broadband radiation detectors in the harsh environments encountered in fusion devices [4]. In a previous paper the authors quantified the ionoluminescence output of the cerium doped alumina ceramic '*Chromox-6*' and determined its light yield for H and He ions respectively [5] to be comparable to that of the widely used scintillator YAP:Ce [6]. One of its main attractions was its ability to tolerate integrated particle fluxes that are several orders of magnitude higher than those withstood by standard powdered phosphors [7]. However, like other ceramics it exhibits

* Corresponding author. Tel.: +34 91 346 6372; fax: +34 91 346 6124.
E-mail address: kieran.mccarthy@ciemat.es (K.J. McCarthy).

0022-3115/$ - see front matter © 2005 Elsevier B.V. All rights reserved.
doi:10.1016/j.jnucmat.2004.12.009

both persistent (or afterglow) and delayed luminescence (i.e. its luminescence output rises gradually for several hundreds of seconds before maximizing) [5,8].

This work is primarily motivated by the application of such radiation-hard luminescent materials in a diagnostic probe, based on the collection of light induced by ions impacting on a thin screen, for measuring fast ion losses, close to the edge of hot plasmas in the TJ-II stellarator [9,10]. In future operations modes, its plasmas will receive up to 2 MW of additional heating from two neutral beam injector (NBI) systems in which neutral hydrogen is accelerated to 40 keV [11] and from which theoretical studies predict that losses due to fast ions could reach 30% of the injected power [12]. To date, diagnostics for detecting fast ion (H^+) losses from the hot plasmas of fusion devices, as well as fast alpha particle losses from D–T fusion devices [13], have employed thin phosphor screens, e.g. ZnS:Ag (P11) [14,15]. However, phosphor powder based screens cannot survive the harsh radiation environment encountered in a fusion device operated for long periods, moreover as such probes must be located close to the plasma outer edge. Here, the search for alternative luminescent materials, with high light output and minimum afterglow, is continued.

Now, in order to quantify the fast ion flux intercepted by a diagnostic ion probe, it is necessary to determine the absolute luminosity of its screen for high-energy ions. Here, absolute ionoluminescence measurements, in terms of photons emitted per incident ion from both the front and back faces, are presented for four candidate materials. The materials, selected because of their availability, radiation hardness, fast response, prior use in fusion diagnostics, or spectral matching to detectors (CCDs, PMTs etc.), are cerium-doped yttrium aluminium garnet ($Y_3Al_5O_{12}$:Ce), commonly known as YAG:Ce, titanium doped alumina (Al_2O_3:Ti), fused silica, and high-purity polycrystalline diamond. In the paper, the experimental set-up, the measurements made with H and He ions having discrete energies between ~50 keV and ~3 MeV and the data analysis employed are described first. Next, quantitative results are summarized and used to estimate light output (i.e. the number of photons per MeV of incident ion energy) and light yields (when possible) which are then compared with known published values. Finally, afterglow, changes in optical absorption, and the suitability of the materials for the application outlined previously, and similar applications, are discussed.

2. Experimental details

2.1. Materials studied

The materials under study, together with some of their principal physical properties, are outlined here. The first is an $Y_3Al_5O_{12}$:Ce (0.15% CeO_2) crystal slice obtained from Crytur Ltd., (Turnov, The Czech Republic). It is a 1 mm thick, 40 mm diameter, screen with a density of 4.57 $g\,cm^{-3}$. The luminescence of Ce^{3+} in $Y_3Al_5O_{12}$ consists of a broad emission that arises from the allowed 5d–4f transition of Ce^{3+} ions and peaks at 550 nm with a stated decay time constant of 70 ns [16]. It has a reported light yield of between 14 and 20.8×10^3 photons MeV^{-1} for samples with different molar concentrations of Ce [17,18] and an α/γ ratio of 0.21 [19]. Also, samples of this material, from another manufacturer, are reported exhibit a 50% decrease in luminescence output after irradiation by $\geqslant 10^{16}$ protons cm^{-2} [20].

The second is an Al_2O_3:$Ti^{3+/4+}$ (0.2% Ti) monocrystalline disk (hexagonal), 1 mm thick and 30 mm in diameter, grown by Crystal Systems Inc. (Salem, MA) using the Heat Exchanger Method (HEM), with its C axis oriented perpendicular to the principal surface [21]. This material is used in broadly tuneable laser sources. The more abundant Ti^{3+} ions ($3d^1$) produce a broad emission band, arising from the ^2E to $^2T_2$ transition, that peaks around 750 nm (well suited to silicon based detectors) while the Ti^{4+} ions emit via charge-transfer transitions in weaker two emission bands centred around 315 and 420 nm [22–24].

The third sample is a 32 mm square, 8 mm thick, fused silica plate, with a density of 2.2 $g\,cm^{-3}$. It was cut from a commercial grade block supplied (99.9%) by Quartz Scientific Inc. (Fairport Harbor, OH). This material was used previously as a broadband bolometric detector in the TJ-I tokamak and when exposed to plasma radiation it produced a dim broad emission spectrum centred about 440 nm [25]. Although fused silica has a low luminescence intensity compared to sapphire, it is still an attractive material as tests have shown it to possess very high damage resistance to neutrons, i.e. little optical damage observed for integrated fluxes up to 6×10^{19} n cm^{-2} [26]. Alternatively, background ionoluminescence could be considered a nuisance for spectroscopy measurements in fusion devices when it is used in vacuum port windows.

The fourth material studied was a high-purity high-quality polycrystalline diamond grown by the chemical vapour deposition (CVD) method using an ellipsoidal reactor at the Fraunhofer Institute (FhG-IAF, Freiburg, Germany) [27]. It was a 1 mm thick, almost transparent, irregular shaped piece (~8 mm wide) with a density of 3.52 $g\,cm^{-3}$. The ionoluminescence of CVD-diamond under MeV proton irradiation is reported to be dominated by three bands that peak around ~4275, ~5170 and ~6200 Å [28].

2.2. Experimental set-up

The measurements were made on the ion beam facility at the Centro Nacional de Aceleradores (Spanish

National Accelerator Centre), Seville, Spain [29]. This facility is based around a 3 MV tandem accelerator (model 9SDH-2 by National Electrostatic Corp., Middleton, WI). For these tests, H^+ ions were created in the SNICS II, a caesium-sputtering source with a TiH_2 cathode, whilst He^+/He^{++} ions were generated by radio frequency within an Alphatross ion source. The resultant ions were then accelerated towards a 90° analysing magnet before passing through a 1 mm by 1 mm collimation entrance slits to the general purpose IBA scattering chamber located at the end of this beam line. In this way fluxes up to 3.5×10^{12} cm^{-2}s^{-1} for protons and up to 2×10^{12} cm^{-2}s^{-1} for He ions were produced on the samples. Next, this chamber was electrically insulated from the accelerator, its pumping system and the visible light detectors. This allowed measurement of the incident beam current by directly connecting the vacuum chamber to a digital current integrator (model 439 by Ortec) in combination with a preset counter (model 2071A by Canberra). The incident ion flux was determined by integrating this current for 120 s (to improve statistics) during sample irradiation with the charge digitiser sensitivity set to 10^{-10} C/pulse. See Fig. 1. The background signal level was determined by repeating this with no beam present. Note also that in the case of He the form of the ion was He^+ for accelerating energies $< \sim 2$ MeV and He^{++} for $\geqslant 2$ MeV. Finally, in order to degrade the ion energy, an aluminised mylar® film (13 μm) fixed on a vacuum indexible holder located inside the IBA chamber was translated into the beam when required. The incident/degraded ion energies are listed in Table 1.

The screens under investigation were placed, in pairs, in an in-house designed vacuum chamber consisting of a

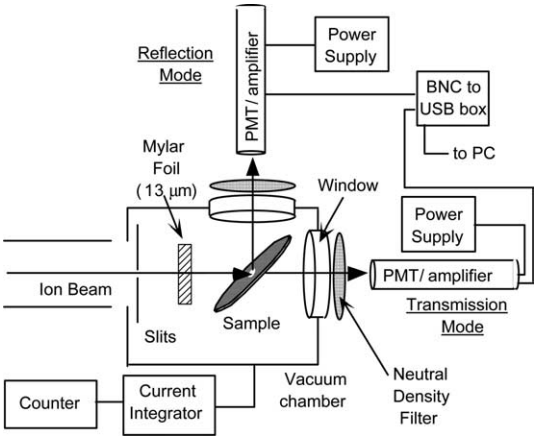

Fig. 1. A schematic diagram of the experimental set-up at CNA showing the sample and photo-multiplier detectors as well as the incident ion beam and light directions. Note that all measurements were made at room temperature.

Table 1
The mean energies of the H and He emerging from the rear of the 13 μm thick aluminised mylar foil as estimated using the SRIM software package [30]

Ion	Incident ion energy (MeV)	Mean energy of emerging ions (keV)	Ion energy straggling (keV) FWHM
H^+	0.84	49	51
He[a]	3.05	46	30

The full-width at half-maximum (FWHM) energy straggling is also given.

[a] The emerging beam consists of approximately 50% neutral He and 50% He^+.

5-way vacuum cross (model CX5-63 by Caburn-MDC, England). This chamber was mounted directly onto the back end of the IBA chamber. The sample pairs were held on the end of a combined rotary and linear motion feed through (model VF-180-3 by Huntington) that was mounted on a second way of the 5-way cross [5]. This system permits measurements to be made at different positions across each sample (to check for any the variation in light output across the sample) as well as at different screen/incident beam angles, i.e. with a sample set at 0° and 45° to the beam. Photomultiplier tubes (PMTs) with integrated signal amplifiers (model H5784-04 by Hamamatsu), mounted on the outside of in-house designed zero-length viewports located at the end of the third and fourth ways, were used to measure the light emitted from the samples. Note that the luminescence light output was measured in both reflection mode, i.e. from the side of the screen facing the incident beam with the sample set at 45° to the ion beam, and transmission mode, i.e., from the rear face of the screen. See Fig. 1. Also, a thin coating of colloidal graphite in water (Aquadag® 18% by Acheson, Plymouth, UK) had been applied to the inside walls of this chamber in order to minimize internal reflections while apertures, located between the sample and detectors, further reduced stray light. Now, in the case of measurements with high light levels, neutral density filters were placed in front of the PMTs. This was preferable to reducing the PMT sensitivity that would have resulted in reduced signal to noise levels. The output signal voltages from the PMTs were fed via a BNC to USB converter box (Series 9800 by Data Translation Inc, Marlboro, MA) to a portable PC where the measured signals were logged and stored. In addition, light flashes were observed occasionally during measurements, these being more frequent at higher energies and for higher ion fluxes (see Fig. 2) and they are attributed to a charge build-up on the irradiated part of the screens (they are good electrical insulators) [14]. These flashes were easily removed when processing the output signals. Finally, once each measurement set had been completed, the beam was blocked, i.e.

switched-off, whilst recording the PMT signal in order to study the decay of the luminescence.

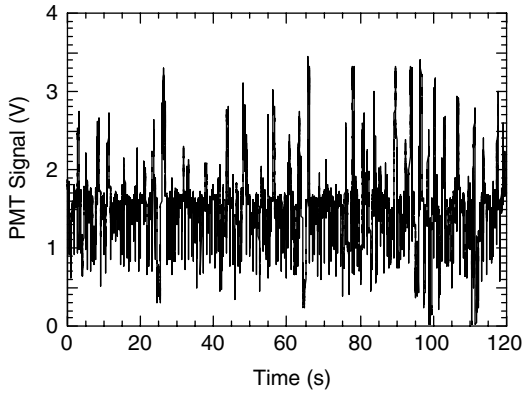

Fig. 2. The output signal from the transmission mode PMT for 2 MeV He^+ incident on the Al_2O_3:Ti screen. The randomly occurring vertical lines are light flashes due to charge build-up on its surface.

3. Results and analysis

3.1. Data analysis

Several steps were required when post-processing the data. First, the ion beam flux incident on a sample was determined for each energy and particle type from the integrated pulse counter reading and the current digitiser sensitivity. Second, the photon fluxes reaching the PMTs were determined from the time integrated light signals (see Fig. 3) using wavelength sensitivity curves provided by the manufacturer [31] while correcting for transmission losses in the vacuum windows, for light attenuation in the neutral density filters (when required) and for signal amplification (fixed at 1 V/μA). Note: the background signals were <0.1% of the light signals. In a posterior test a difference was spotted in the outputs of the two PMTs used when illuminated by a fixed light source. Hence, tests were repeated with several PMTs (same model) to determine a mean signal level so that corrections could be applied to the sensitivity curve for the two PMTs. Third, by taking account of the cera-

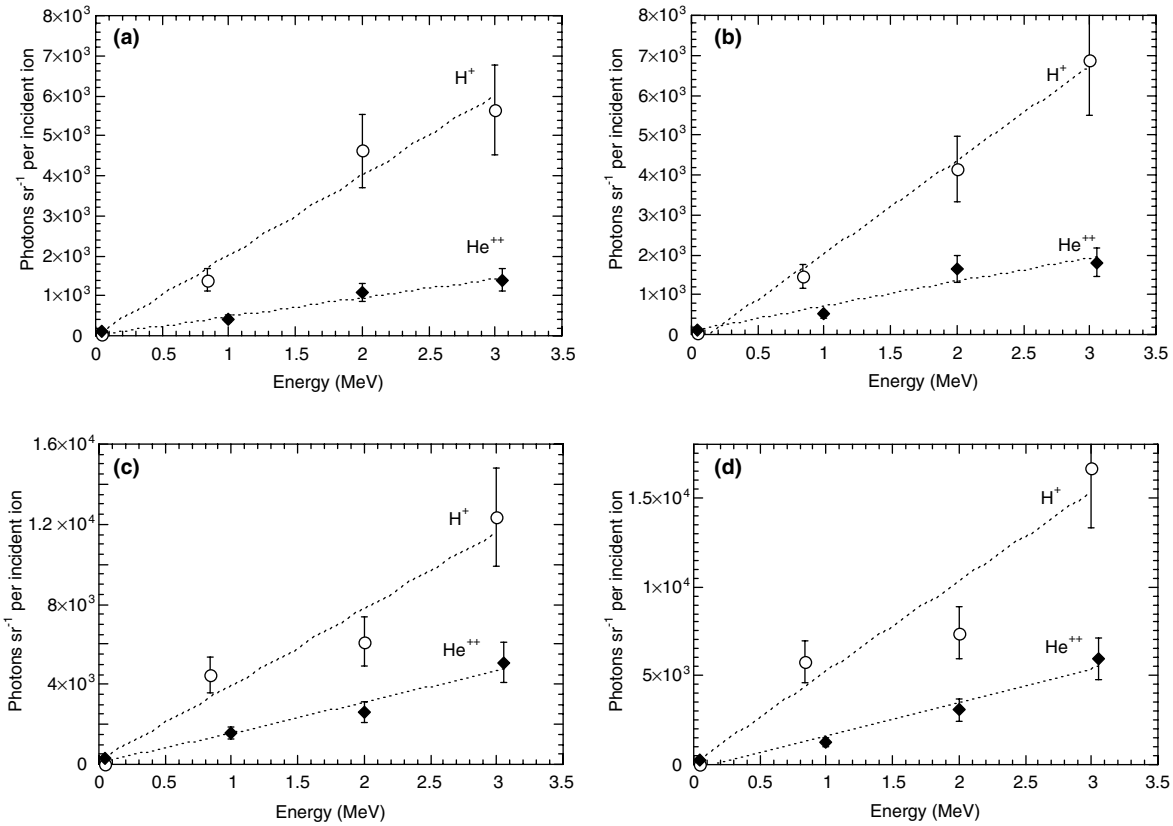

Fig. 3. Plots of the number of visible photons emitted per steradian per incident H^+ and $He^{+/++}$ ion as a function of ion energy for emission normal to the screen surface. These are (a) YAG:Ce transmission mode, (b) YAG:Ce reflection mode, (c) Al_2O_3:Ti transmission mode, (d) Al_2O_3:Ti reflection mode, (e) fused silica transmission mode, (f) fused silica reflection mode, and (g) CVD transmission mode.

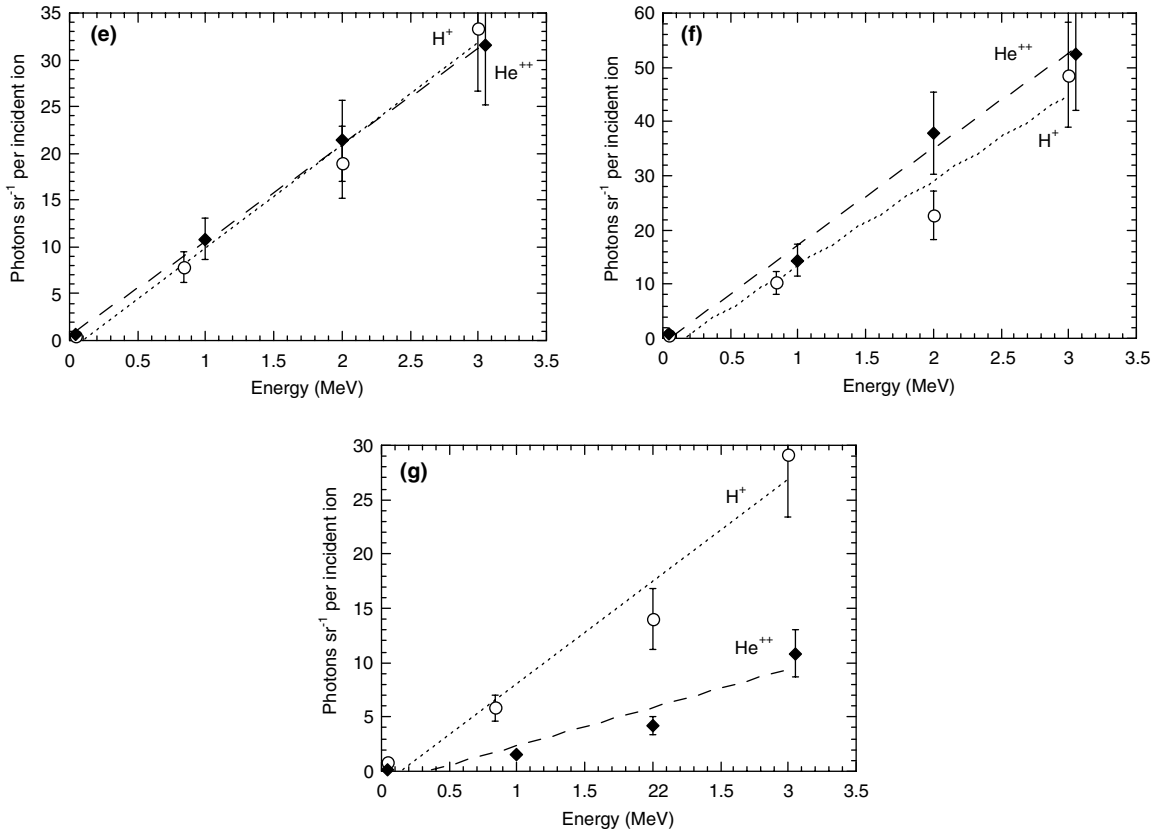

Fig. 3 (*continued*)

mic/PMT geometry, the number of photons emitted normal to the screen surface(s) per steradian was determined. As the screen to PMT separation was ~151.5 mm, the beam spot area (~1 mm^2) constituted a point source except in the case of keV energies where they constituted an extended source due to angular straggling of the beam as it traversed the mylar® film. In this case the fractional solid angle to the detector was obtained using equations described in Ref. [32] for disk sources which result in a fixed error of ~1% for absolute measurements.

3.2. Absolute luminosity and light yield

Next, in Fig. 3, the visible photon flux emitted per steradian (normal to a screen surface) per incident ion is plotted as a function of particle type and energy for each screen and for both transmission and reflection mode. Note that for transmission mode the photon flux has not been corrected for transmission or internal reflection losses. It is estimated that these measurements can be reproduced to within 10% with a relative uncertainty below 20%. The most significant sources of absolute uncertainty include the response of the H5783-04 PMT, ±10%, and the ion beam current, ±10%. Now, charged particles such as protons or α particles lose energy through Coulomb interaction with electrons in a solid. For weakly penetrating particles the rate of energy loss increases as the mass of the particle increases, whereas the luminescence yield decreases [33]. For particles with equal energies, a He ion will produce 0.2–0.4 times the light produced by H^+. Here, this factor lies within this range for three of the materials (i.e. ~0.3 for YAG:Ce, ~0.38 for Al_2O_3:Ti, and ~0.34 for the CVD-diamond) but is between ~0.8 and unity in the case of the silica.

It is apparent from Fig. 3 that the ionoluminescence from the YAG:Ce and Al_2O_3:Ti screens is several orders of magnitude higher than that from the fused silica and CVD-diamond screens. Hence, for the intended application, the signal levels in probes employing either YAG:Ce or Al_2O_3:Ti as incident ion to light transducers should not be signal limited. Generally, the efficiency of luminescent materials is compared in terms of light yield, i.e. the number of photons created per incident MeV of energy (usually γ-ray) after correcting for internal light attenuation and reflection. In order to compare these measurements with others, it is first necessary to

Table 2
The light output from the back (transmission mode) and front (reflection mode) faces of the screens under study when irradiated by H and He ions accelerated to keV and MeV energies

Material	Mode	Light output for H^+ (photons MeV^{-1})	Light output for He^{++} (photons MeV^{-1})
YAG:Ce (0.15% CeO_2)	Transmission	6.43×10^3	1.53×10^3
YAG:Ce (0.15% CeO_2)	Reflection	7.16×10^3	2.06×10^3
Al_2O_3:Ti	Transmission	1.24×10^4	5.01×10^3
Al_2O_3:Ti	Reflection	1.63×10^4	5.8×10^3
Fused silica	Transmission	3.43×10^1	3.35×10^1
Fused silica	Reflection	5.65×10^1	4.77×10^1
CVD-diamond	Transmission	2.83×10^1	1.0×10^1

consider the Lambertian fall-off in light intensity as a function of angle to the surface normal in order to estimate the photon output from each face per MeV incident. See Table 2. From this, an estimate of the light yield can made by assuming it to be double that of the light output for reflection mode and by correcting for the α/γ ratio where available. This is reasonable, as the ions are stopped close to the surface and undergo little self-absorption, although it may result in a slight underestimation. See Table 2 again. Indeed, the resultant estimated YAG:Ce (0.15% $Ce0_2$) light yield, i.e. 19.6×10^3 photons MeV^{-1} is in close agreement with previously reported upper-limit values [17]. However, in the case of Al_2O_3:Ti (0.2%), no published α/γ ratios or ionoluminescence measurements have been found so direct light yield comparisons are difficult. Nonetheless, the light yield of this sample must be $\gg 11.6 \times 10^3$ photons MeV^{-1} (estimated using $\alpha/\gamma = 1$), which is considerably higher than that published for a sample with a 0.07% Ti concentration, i.e. 14% that of CsI:Tl (or $\sim 8 \times 10^3$ photons MeV^{-1}) [34]. Other authors have shown, using relative photoluminescence measurements, that the light output increases as Ti concentration is increased before rolling-off above concentrations of ~0.3% Ti [35]. These findings imply that Al_2O_3:Ti (0.2%) should have a high light yield, a result that is very promising for scintillators with high output in the long wavelength region where silicon based detectors have their peak sensitivities. For comparison, the light yield of the well known scintillator CsI(Tl) is $\sim 60 \times 10^3$ photons MeV^{-1} [6].

3.3. Afterglow

The evolution of the luminescence output from the screens after blocking the ion beam, i.e. *switched-off*, is summarized in Fig. 4. In the case of the YAG:Ce and silica samples the afterglow observed was insignificant, i.e. it could not be distinguished from the closing time of the shutter, and these are not shown. However persistent afterglow was observed from the Al_2O_3:Ti sample after it had been irradiated for several minutes by H^+ and $He^{+,++}$ ions accelerated to MeV energies (i.e. after performing various 120 s long measurements). See Fig. 4. Note that after irradiating the same sample for shorter periods, i.e. a few tens of seconds, the afterglow was considerably reduced. In order to understand this it is useful to consider ceramics that show considerable afterglow after X-ray irradiation and the source of afterglow is explained by the fact that some of the electrons created by the X-rays are trapped by vacancies in the host whereas the holes are trapped by the dopant ions [36]. The electrons recombine with these holes after thermal detrapping thereby yielding delayed luminescence. It is hypothesised here that when irradiated for a long period by a high flux beam the trap/hole density in the Al_2O_3:Ti becomes sufficiently high so as to produce significant delayed luminescence. When irradiated for shorter periods or with a lower flux beam, the trap/hole density is lower and the resultant afterglow is also lower. However, a deeper study of this is beyond the scope of this work as it is considered that the afterglow from Al_2O_3:Ti does not impair its use in a fast-ion loss probe for determining integrated ion fluxes.

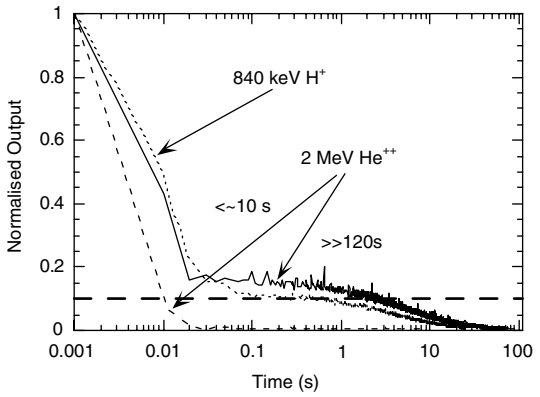

Fig. 4. The temporal evolution of luminescence (normalized) from the Al_2O_3:Ti sample after beam *switch-off* (at $t = 0$ s) when irradiated by 840 keV H^+ for several minutes, by 2 MeV He^{++} for several minutes, and by 2 MeV He^{++} for several seconds. The ion flux was between 1 and 2×10^{12} $cm^{-2}s^{-1}$ for these tests.

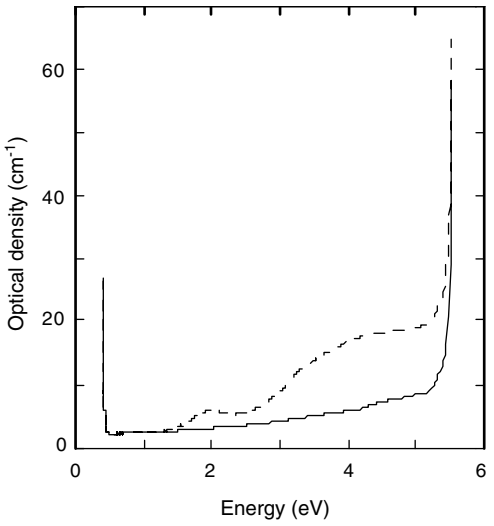

Fig. 5. Optical absorption spectra of the CVD-diamond sample before (continuous line) and after (broken line) the experiment. These were obtained with a Cary 5 spectrophotometer by Varian (Palo Alto, CA).

3.4. Irradiation effects on the CVD-diamond

Fig. 5 shows optical absorption spectra of the CVD-diamond obtained before and after these ionoluminescence measurements. In the first spectrum no significant optical absorption band is observed except for the gap-related rise around 5.5 eV and the well-known IR absorption band [37]. After ion irradiation a brown colouring of the sample was clearly observed, this being related to the optical absorption bands seen in Fig. 5 around 2 and 4 eV (6200 and 3100 Å). Their origin is not clear, but taking into account the low ion (implantation) dose ($\sim 10^{15}$ ions cm^{-2}), they may be related to changes in the charge state of previously existing defects. These bands can have an important effect on absolute ionoluminescence due to increased absorption. Indeed the light output was observed to change from white (at the start of the experiment) to green (at the end). Finally, no colour changes or darkening were seen in the other samples studied.

4. Conclusions

The absolute ionoluminosity of several materials for low mass ions (H^+, He^+) accelerated to keV and MeV energies have been determined. The results presented indicate that the signal levels from fast ion loss probes employing either the YAG:Ce or Al_2O_3:Ti as incident ion to light transducers will not be signal limited, and that afterglow will not be a serious problem.

Acknowledgements

This work was partially funded by the Spanish 'Ministerio de Ciencia y Tecnología' (MCyT) under Grant No. FTN2003-0905 and D.J.R. is supported by a scholarship BES-2004-4771 as part of the same programme. J.G.L. acknowledges the '*Ramon y Cajal*' program of the MCyT for financial support. The CVD-diamond sample was kindly supplied by Dr R. Heidinger.

References

[1] C.D. Johnson, European Laboratory for Particle Physics Report CERN/PS/90-42(AR).
[2] S. Yencho, D.R. Walz, IEEE Trans. Nucl. Sci. NS 32 (1985) 2009.
[3] A.H. Lumpkin, B.X. Yang, W.J. Berg, M. White, J.W. Lewellen, S.V. Milton, Nucl. Instrum. and Meth. A 429 (1999) 336.
[4] A. Baciero, B. Zurro, K.J. McCarthy, P. Martín, M.C. de la Fuente, Rev. Sci. Instrum. 73 (2002) 283.
[5] K.J. McCarthy, J. García López, F. Martín Hernández, B. Zurro, A. Baciero, M.A. Respaldiza, J. Nucl. Mater. 321 (2003) 78.
[6] M. Moszynski, M. Kapusta, M. Mayhugh, D. Wolski, S.O. Flyckt, IEEE Trans. Nucl. Sci. 44 (1997) 1052.
[7] W.A. Hollerman, J.H. Fisher, L.R. Holland, J.B. Czirr, IEEE Trans. Nucl. Sci. 40 (1993) 1355.
[8] S.D. Borovkov, S.A. Grishenkov, V.S. Konevskii, E.V. Krivonosov, L.A. Litvinov, V.P. Novikov, E.V. Serga, A.V. Kharlamov, Pribory i Teknika Éksperimenta 4 (1991) 33.
[9] C. Burgos, B. Zurro, J. Guasp, M.A. Ochando, K.J. McCarthy, F. Medina, A. Baciero, M. Liners, C. Fuentes, Rev. Sci. Instrum. 74 (2003) 1861.
[10] E. Ascasíbar et al., Fusion Eng. Des. 56&57 (2001) 145.
[11] J. Guasp, M. Liniers, C. Fuentes, G. Barrera, Fusion Technol. 35 (1999) 32.
[12] J. Guasp, M. Liniers, Fusion Technol. 34 (1993) 251.
[13] S.J. Zweben, R.L. Boivin, C.-S. Chang, G.W. Hammett, H.E. Mynick, Nucl. Fusion 31 (1991) 2219.
[14] D.S. Darrow, A. Werner, A. Weller, Rev. Sci. Instrum. 72 (2001) 2936.
[15] M. Isobe, D.S. Darrow, T. Kondo, M. Sasao, K. Toi, M. Osakabe, H. Shimizu, Y. Yoshimura, C. Takahashi, S. Murakami, S. Okamura, K. Matsuoka, Rev. Sci. Instrum. 70 (1999) 827.
[16] http://www.crytur.cz/scintillator.htm.
[17] M. Moszynski, T. Ludziejewski, D. Wolski, W. Klamra, L.O. Norlin, Nucl. Instrum. and Meth. A 345 (1994) 461.
[18] S. Majewski, C. Zorn, in: E. Sauli (Ed.), Symp. on Instr. in High Energy Physics, World Scientific, 1992.
[19] T. Ludziejewski, M. Moszynski, M. Kapusta, D. Wolski, W. Klamra, K. Moszynska, Nucl. Instrum. and Meth. A 398 (1997) 287.
[20] W.A. Hollerman, S.W. Allison, S.M. Goedeke, P. Boudreaux, R. Guidry, E. Gates, IEEE Trans. Nucl. Sci. 50 (2003) 754.

[21] www.crystalsystems.com.
[22] W.C. Wong, D.S. McClure, S.A. Basun, M.R. Kokta, Phys. Rev. B 51 (1995) 5693.
[23] B.D. Evans, J. Lumin. 60&61 (1994) 620.
[24] A.I. Surdo, V.S. Kortov, F.F. Sharafutdinov, Radiat. Prot. Dosimetry 84 (1999) 261.
[25] B. Zurro, C. Pardo, J.L. Alvarez Rivas, J. Phys. D: Appl. Phys. 19 (1986) 1895.
[26] A. Gorshkov, D. Orlinski, V. Sannikov, K. Vukolov, S. Gonchararov, Y. Sadovnikov, A. Kirillov, J. Nucl. Mater. 273 (1999) 271.
[27] www.iaf.fraunhofer.de.
[28] C. Manfredotti, E. Vittone, A. Lo Giudice, C. Paolini, F. Fizzotti, G. Dinca, V. Ralchenko, S.V. Nistor, Diamond Relat. Mater. 10 (2001) 568.
[29] J. García López, F.J. Ager, M. Barbadillo Rank, F.J. Madrigal, M.A. Ontalba, M.A. Respaldiza, M.D. Ynsa, Nucl. Instrum. and Meth. B 161–163 (2000) 1137.
[30] http://www.srim.org/.
[31] Hamamatsu Photonics K.K. (1996), Photosensor Module H5783 Series, Technical data sheet (TPMHB0293EA) Shizuoka-ken, Japan.
[32] N. Tsoulfanidis, in: Measurement and Detection of Radiation. McGraw-Hill Series in Nuclear Engineering, Hemisphere Publishing Corporation, Washington, 1983.
[33] G. Blasse, B.C. Grabmaier, Luminescent Materials, Springer, Berlin, 1994.
[34] P.A. Rodnyi, E.I. Gorohova, S.B. Mikhrin, A.N. Mishin, A.S. Potapov, Nucl. Instrum. and Meth. A 486 (2002) 244.
[35] J.C. McCallum, L.D. Morpeth, Nucl. Instrum. and Meth. B 148 (1999) 726.
[36] G. Blasse, J. Alloys Compd. 255 (1995) 529.
[37] K. Iakoubovskii, G.J. Adriaenssens, Diamond Relat. Mater. 9 (2001) 568.